

**Environmental and vegetation drivers of seasonal CO<sub>2</sub> fluxes in a sub-Arctic forest-mire ecotone**

Rafael Poyatos<sup>\* a, b</sup>, Andreas Heinemeyer<sup>c</sup>, Phil Ineson<sup>c</sup>, Jonathan G. Evans<sup>d</sup>, Helen C. Ward<sup>d</sup>, Brian Huntley<sup>b</sup> and Robert Baxter<sup>b</sup>

<sup>a</sup> CREAF, Cerdanyola del Vallès 08193, Spain

<sup>b</sup> School of Biological and Biomedical Sciences, Durham University, Durham DH1 3LE, UK.

<sup>c</sup> Environment Department, Stockholm Environment Institute, University of York, York YO10 5DD, UK

<sup>d</sup> Centre for Ecology and Hydrology, Wallingford, Oxfordshire, UK

\*Corresponding author: r.poyatos@creaf.uab.es

**Short title: CO<sub>2</sub> fluxes in a sub-Arctic forest-mire ecotone**

R.P. conceived and designed the study, performed research, analysed data and wrote the paper; A.H conceived and designed the study and revised the paper; P. I conceived and designed the study and revised the paper; J.G.E. performed research, analysed data and revised the paper; H.C.W performed research, analysed data and revised the paper; B.H. conceived and designed the study and revised the paper; R.B. conceived and designed the study and revised the paper;

## Abstract

Unravelling the role of structural and environmental drivers of gross primary productivity (GPP) and ecosystem respiration ( $R_{eco}$ ) in highly heterogeneous tundra is a major challenge for the upscaling of chamber-based CO<sub>2</sub> fluxes in Arctic landscapes. In a mountain birch woodland-mire ecotone, we investigated the role of LAI (and NDVI), environmental factors (microclimate, soil moisture) and microsite type across tundra shrub plots (wet hummocks, dry hummocks, dry hollows) and lichen hummocks, in controlling net ecosystem CO<sub>2</sub> exchange (NEE). During a growing season, we measured NEE fluxes continuously, with closed dynamic chambers, and performed multiple fits (one for each three-day period) of a simple light and temperature response model to hourly NEE data. Tundra shrub plots were largely CO<sub>2</sub> sinks, as opposed to lichen plots, although fluxes were highly variable within microsite type. For tundra shrub plots, microsite type did not influence photosynthetic parameters but it affected basal (i.e., temperature-normalised) ecosystem respiration ( $R_0$ ). PAR-normalised photosynthesis ( $P_{600}$ ) increased with air temperature and declined with increasing vapour pressure deficit.  $R_0$  declined with soil moisture and showed an apparent increase with temperature, which may underlie a tight link between GPP and  $R_{eco}$ . NDVI was a good proxy for LAI, maximum  $P_{600}$  and maximum  $R_0$  of shrub plots. Cumulative CO<sub>2</sub> fluxes were strongly correlated with LAI (NDVI) but we observed a comparatively low GPP/LAI in dry hummocks. Our results broadly agree with the reported functional convergence across tundra vegetation, but here we show that the role of decreased productivity in transition zones and the influence of temperature and water balance on seasonal CO<sub>2</sub> fluxes in sub-Arctic forest-mire ecotones cannot be overlooked.

**Key-words:** carbon balance, ecosystem respiration, gross primary productivity, leaf area index, lichen, NDVI, net ecosystem exchange, soil moisture, transition zones, tundra

## Introduction

Arctic mires and tundra ecosystems store large amounts of C (Turunen and others, 2002; Limpens and others, 2008) and are experiencing shifts towards more productive vegetation as climate at high-latitudes becomes warmer (Beck and others, 2011; Elmendorf and others, 2012). Climate-driven shifts in net ecosystem CO<sub>2</sub> exchange (NEE) of Arctic tundra are highly relevant for carbon-climate feedbacks at the global scale, especially under the enhanced warming predicted for the Arctic (Christensen and others, 2007). On one hand, warmer conditions may enhance gross primary productivity (GPP) through the alleviation of thermal constraints on photosynthesis, changes in species composition and/or the increase of growing season length and nutrient availability (Natali and others, 2012). On the other hand, higher temperatures and associated hydrological changes may increase ecosystem respiration ( $R_{eco}$ ) (Dorrepaal and others, 2009) and even release old C stored in permafrost soil and peat (Schuur and others, 2009), potentially offsetting any productivity increases.

Annual sums of ecosystem CO<sub>2</sub> fluxes have shown that NEE is typically negative (i.e. net C uptake by the ecosystem) in northern mires (Lund and others, 2010). During warm and dry years, however, sink strength generally decreases and mires can turn into

net carbon sources (Alm and others, 1999) because of increases in  $R_{eco}$ , declines in GPP, or both (Moore and others, 2002; Bubier and others, 2003). Hence, the relative sensitivities of GPP and  $R_{eco}$  to temperature, growing season length and substrate water content will determine the climate-induced changes in NEE of high latitude mires and tundra ecosystems. These responses will likely vary across ecosystem types, moisture gradients and microtopographic positions (Oberbauer and others, 2007), which can vary considerably on spatial scales of meters or less in spatially complex Arctic landscapes (Asner and others, 2003; Spadavecchia and others, 2008).

This heterogeneity of high-latitude low-stature vegetation results in a marked spatial variability of NEE and its flux components associated to microtopography, local hydrology (Heikkinen and others, 2004; Nobrega & Grogan, 2008; Pelletier and others, 2011) and community composition (Riutta and others, 2007). However, functional convergence of canopy N-use across Arctic vegetation types (Van Wijk and others, 2005) results in GPP being largely explained by microclimate and leaf area index (LAI) alone (Shaver and others, 2007; Street and others, 2007). In these ecosystems, the observed normalised difference vegetation index (NDVI), a good surrogate of LAI, and hence of GPP at given environmental conditions, is often also a good predictor of measured  $R_{eco}$  (McMichael, 1999; Boelman and others, 2003). However, whether these relationships between LAI (NDVI) and  $CO_2$  exchange also hold for integrated fluxes over the entire growing season has not been thoroughly tested (but see Marushchak and others (2013)).

Landscape-level studies of CO<sub>2</sub> fluxes in tundra and mire ecosystems depict a pronounced seasonal variability in NEE and its components (Lindroth and others, 2007; Lund and others, 2010). At a finer spatial scale, seasonal variation in CO<sub>2</sub> fluxes is high (Bubier and others, 2003) and responses to environmental drivers may be ecosystem-specific (Nobrega & Grogan, 2008). Because of this high spatial and temporal variability, detailed measurements across time at multiple points in space are critical for understanding the magnitude and variability of CO<sub>2</sub> exchange in different vegetation and ecosystem types for point-to-landscape scaling efforts (Stoy and others, 2013; Oechel and others, 1998; Soegaard and others, 2000).

The margins of mires at the mountain birch (*Betula pubescens* ssp. *czerepanovii* (Orlova) Hamet-Ahti) woodland-tundra ecotone in northern Fennoscandia are highly representative of heterogeneous low-arctic vegetation. Here, the formation of cryogenic earth hummocks results in a complex microtopography and thus a variety of habitats that differ in snow cover during the winter and substrate moisture during the growing season (Van Vliet-Lanoe & Seppala, 2002). In this study, we used an automated chamber system to measure hourly NEE across a mire-mountain birch woodland ecotone in northern Finland. We focused on differences on NEE controls across four microsites: three tundra shrub microsites, differing in microtopographic position and soil moisture, and one lichen microsite. Fluxes were modelled using semi-empirical responses to light and temperature, yielding normalised GPP at PAR=600  $\mu\text{mol m}^{-2} \text{s}^{-1}$  ( $P_{600}$ ) and  $R_{eco}$  normalised to an air temperature of 0°C (basal ecosystem respiration,  $R_0$ ). These and other parameters associated with diel environmental controls on NEE

were analysed in relation to seasonal variation in environmental drivers (mainly microclimate and soil moisture) and plant structure obtained from LAI harvests and seasonal hand-held NDVI measurements. We hypothesised that: (H1a) NDVI would be a good surrogate for LAI and (H1b) would explain differences in  $P_{600}$  across microsites. It was also postulated that (H2) for tundra shrub microsites, seasonality in photosynthetic parameters would be unaffected by microsite type and would be largely explained by NDVI and air temperature (H3a). We also hypothesised that  $R_0$  would be positively related to NDVI and, given the prevailing wet conditions in sub-Arctic mires,  $R_0$  would decline with soil moisture because of limited oxygen diffusion into the soil (H3b). According to the functional convergence reported for tundra vegetation (H4) growing season cumulative NEE would be strongly correlated with LAI (or NDVI) across microsites.

## Methods

### *Study site and plot characteristics*

The study area (69°29'35.37"N, 27°13'52.91"E, 272 m.a.s.l.) was located near Petsikko, ca. 35 km south of the Kevo Subarctic Research Institute in northern Finland. Mean annual temperature at Kevo (80 m.a.s.l.) is -1.6 °C and annual precipitation is 415 mm (1962-2007, Kevo Subarctic Research Institute). The mineral soil is formed by glacial till and underlain by gneiss. The site presents topographical depressions occupied by open water, gradually turning to *Eriophorum-Carex* lawns and *Sphagnum* pools at the

mire (peatland) margins. The surrounding gentle slopes are mostly covered by mesic tundra shrubs growing on peat deposits, grading into a sparse mountain birch (*Betula pubescens ssp. czerepanovii*) woodland.

We studied a forest-mire ecotone (Appendix 1 in Online publication), characterised by hummocks with a typical height of *ca* 0.6 m and a maximum diameter of *ca.* 1 m. The mean depth of the organic horizon was *ca.* 20 cm (Wayolle, 2011). Ecotones between mires and sub-Arctic woodland in northern Fennoscandia display characteristic formations of peat hummocks, associated with the area of discontinuous permafrost (Van Vliet-Lanoe & Seppala, 2002). Even though there is no permafrost at the site, these hummocks can show ice lenses in their cores even in late summer (Wayolle, 2011) and are usually covered by various shrubs, mosses and lichens. The shrubs were dominated by mesic tundra heath species, such as *Empetrum nigrum* L., *Vaccinium vitis-idaea* L., *Calluna vulgaris* L. (Hull) and *Vaccinium myrtillus* L. The moss species included *Sphagnum fuscum* (Schimp.) Klinggr., *Pleurozium schreberi* (Brid.) Mitt., and acrocarpous mosses. The lichens (*Cetraria* spp. and *Cladonia* spp.) form a thin cryptogamic crust covering tall hummock tops devoid of vascular vegetation because of frost exposure and wind abrasion (Van Vliet-Lanoe & Seppala, 2002).

We deployed 12 PVC collars (19.9 cm internal diameter and 4.5 cm height) in early June 2008 to measure four microsite types, with three replicates for each type (Table 1). Three microsite types were dominated by tundra shrubs and differed in their spatial location, both in terms of microtopography and position along the mire to forest

ecotone: mire hummocks (HM) were located close to the wetland and forest hummocks (HF) were nearer the forest edge and dry hollows (DH) occupied depressions at intermediate locations. HM and HF were dominated by *E. nigrum* and *Vaccinium* species, and DH was almost exclusively covered by *C. vulgaris*. Lichen hummocks (HL) had only a poor lichen and moss cover (Table 1). Given their similar shrub vegetation characteristics, HM, HF and DH microsites will hereafter be referred to as ‘tundra shrub microsites’ throughout the manuscript.

#### *Multiplexed automated CO<sub>2</sub> flux measuring system*

We used a closed dynamic CO<sub>2</sub> flux system for measuring CO<sub>2</sub> flux rates ( $\mu\text{mol CO}_2 \text{ m}^{-2} \text{ s}^{-1}$ ). The system comprised an infra-red gas analyser (Li-Cor 8100, Li-Cor Inc., Lincoln, Nebraska, USA), a custom-built multiplexed gas handler unit (Electronics Workshop, Biology Department, University of York, UK) and 12 clear, Perspex chambers based on a commercial soil respiration model (LiCor 8100-101; 20 cm diameter). Chambers closed and opened sequentially, allowing hourly measurement cycles of 12 vegetation patches at a maximum radial distance of 20 m from the multiplexer. The chamber bases had rims with a rubber gasket, which ensured a tight fit with PVC collars. These collars were deployed on the 12 selected patches and gently sealed to the ground, without cutting or inserting into the substrate, using non-setting plumber’s putty (Plumber’s Mait, Bostik Ltd., Leicester, UK). We took this precaution to avoid damaging the prostrate stems and the roots of dwarf-shrub tundra species, which could potentially affect measured C fluxes as shown for another peatland



(Heinemeyer and others, 2011). The system operated from the 11<sup>th</sup> of June (DOY 163) until the 14<sup>th</sup> of September (DOY 258) of 2008. Further details on the operation of a similar system used for respiration measurements can be found in Heinemeyer and others (2011).

We used the meteorological sign convention for NEE, in which a net flux from the atmosphere to the biosphere is negative. NEE was calculated as:

$$NEE = -\frac{PV}{ART_0} \frac{d}{dt} [CO_2]_{dry} \quad \text{Eq. 1}$$

where  $P$  is air pressure inside the chamber (Pa),  $V$  (m<sup>3</sup>) is the system volume in (chamber, irga/multiplexer and tubing),  $T_0$  (°C) is air temperature at chamber closure,  $R$  (J K<sup>-1</sup>μmol<sup>-1</sup>) is the ideal gas constant,  $A$  is chamber surface area (m<sup>2</sup>) and  $d[CO_2]_{dry}/dt$  (μmol mol<sup>-1</sup> s<sup>-1</sup>) is the rate of change in water vapour-corrected CO<sub>2</sub> concentration in the chamber headspace. We calculated this rate from CO<sub>2</sub> and water vapour concentrations measured every 2 seconds, over the 150 s period when the chamber remained closed. We estimated  $d[CO_2]_{dry}/dt$  from the first order term of a quadratic fit between  $[CO_2]_{dry}$  and time since chamber closure. Nonlinear fits describe better the concentration dynamics in the closed chamber, and do not systematically underestimate the fluxes (Kutzbach and others, 2007). However, in the presence of noisy concentration data under low flux conditions, we opted for the more stable linear fit; we selected the linear regression whenever the slope for the linear fit and the linear term of the quadratic fit had opposite signs.

We took pictures of all the plots with a digital camera (DX 7630, Eastman Kodak, Rochester, NY, USA) on the 31st of July 2008, and estimated percentage cover for each species combining manual delimitation with the ‘selection by colour’ tool in the image analysis software GIMP v. 2.4.6. At the end of the flux measurement period (16<sup>th</sup> of September), we harvested all the aboveground biomass inside the collars, dried it for 48 h at 60°C and weighed it. Leaf biomass for each plot was converted into leaf area using specific leaf area (SLA) measured for each species in nearby plots (Fletcher, Sloan & Phoenix, unpublished), summed up and calculated plot-scale LAI (Table 1).

We measured NDVI on the study plots on seven dates (29<sup>th</sup> June, 2<sup>nd</sup> July, 31<sup>st</sup> July, 8<sup>th</sup> August, 1<sup>st</sup> September, 6<sup>th</sup> September, and 11<sup>th</sup> September). We used a two-channel sensor (SKR 1800, Skye Instruments) attached to a hand-held console (SpectroSense2, Skye Instruments) to measure surface reflectance in the red (channel 1, 0.56-0.58 nm) and near-infrared (channel 2: 0.725-1.1 nm) bands. We held the sensor pair at a height of 0.4 m above the plot, so that the effective area measured by the sensor measuring reflected light (25° field of view, no diffuser cap attached) corresponded to the collar area. We used the diffuser cap to cosine-correct the incident light measured by the upward-looking sensor. NDVI was linearly interpolated across measuring dates in order to obtain a continuous daily estimate. For our plots, dominated by evergreen species (Table 1), this interpolation was a reasonable approximation after checking NDVI variation measured from a nearby tower-mounted sensor (J. Evans, unpublished results).

## *Environmental measurements*

We measured photosynthetically active radiation (PAR) with a pair of quantum sensors (Delta-T, Burwell, UK); one was deployed inside one of the collars and the other just outside the same collar. We thus quantified a *ca.* 20% PAR attenuation during chamber closure by fitting a power function between ambient and inside-chamber PAR ( $\text{PAR}_{\text{ambient}} = 0.80 \cdot \text{PAR}_{\text{chamber}}^{1.01}$ ;  $R^2 = 0.97$ ;  $N = 945$ ). We used this function to correct ambient PAR to inside-chamber values (needed to correct for ambient NEE fluxes).

We obtained plot-specific air temperature from the value measured by chamber thermistors at chamber closure. We calculated vapour pressure deficit (VPD) using air temperature and relative humidity in the chamber (Jones, 1992). Site air temperature, PAR and precipitation were measured in a meteorological tower at *ca.* 50 m from the location of the chambers. We measured half-hourly volumetric soil moisture (SWC; CS616 water content reflectometer and CR1000 datalogger, Campbell Scientific, UK) in one representative plot of each vegetation type ( $N = 4$ ). We installed the reflectometer rods (30 cm long) obliquely so that the measurement was representative of a larger area; measuring depth was thus 0-10 cm. We also measured soil temperature (5 cm depth) (every 30 min) in all plots by soil thermistors connected to a datalogger (DL2e, Delta-T Devices, Cambridge, UK).

## *NEE modelling*

254

255 We modelled plot-scale CO<sub>2</sub> fluxes using semi-empirical responses to light and  
256 temperature. We binned hourly daytime NEE fluxes in 3-day classes and fitted the  
257 following model, which combines a rectangular hyperbola to simulate GPP and an  
258 exponential relationship between ecosystem respiration and temperature (Williams and  
259 others, 2006):

260

261 
$$NEE = R_0 e^{\beta T} - \frac{P_{max} PAR}{k + PAR}$$
 Eq. 2

262

263 Where  $R_0$  is basal respiration ( $\mu\text{mol CO}_2 \text{ m}^{-2} \text{ s}^{-1}$ ), representing ecosystem respiration at  
264 0 °C,  $\beta$  ( $^{\circ}\text{C}^{-1}$ ) is respiration sensitivity to temperature,  $P_{max}$  ( $\mu\text{mol CO}_2 \text{ m}^{-2} \text{ s}^{-1}$ ) is  
265 asymptotic maximum photosynthesis and  $k$  is the half-saturation constant ( $\mu\text{mol PAR}$   
266  $\text{m}^{-2} \text{ s}^{-1}$ ). For comparative purposes, we calculated gross photosynthesis at  $\text{PAR} = 600$   
267  $\mu\text{mol m}^{-2} \text{ s}^{-1}$  ( $P_{600}$ ) (Street and others, 2007), we expressed respiration sensitivity to  
268 temperature as a  $Q_{10}$  coefficient ( $Q_{10}=e^{\beta}$ ) and we converted  $k$  to quantum efficiency ( $\alpha=$   
269  $P_{max}/k$ ;  $\mu\text{mol CO}_2 \mu\text{mol}^{-1} \text{ PAR}$ ) (Atkin and others, 2005; Street and others, 2007).

270

271 Despite some gaps due to power failures in this remote and harsh environment, we  
272 obtained CO<sub>2</sub> time series that covered 51-58% of the hourly intervals within the  
273 measuring period, depending on the plot (*cf.* Results). Therefore, the parameters of the  
274 NEE model were linearly interpolated to complete missing days and then the model was

applied to gap-fill the NEE time series. The same model was also used to decompose NEE into GPP and  $R_{eco}$ . The completed CO<sub>2</sub> flux time series were then aggregated into growing season cumulative values.

## *Data analyses*

All data analyses, including CO<sub>2</sub> flux calculations, were carried out using the statistical package R 2.9 (R Development Core Team, 2009). We calculated the 5% and 95% quantiles of NEE hourly rates (NEE<sub>5%</sub> and NEE<sub>95%</sub>, respectively) for each plot, to represent robust estimates of sustained, maximum CO<sub>2</sub> uptake and release capacity and to aid in comparative analyses across vegetation types. Linear mixed-effects models (Pinheiro & Bates, 2000) were used to analyse the influences of environmental drivers and structural variables on the seasonal dynamics of NEE model parameters. Models were fitted using restricted maximum likelihood (package lme, R 2.9), with plot code introduced as a random factor. We tested all possible combinations of time (DOY), environmental drivers (air temperature, VPD and soil moisture) and structural variables (NDVI, vegetation type) as fixed effects. As the NEE model parameters are subject to temporal autocorrelation we introduced a correlation structure based on a continuous first-order autoregressive process (corCAR1). Model performance was assessed via graphical inspection of the residuals and their autocorrelation function. Models with the lowest Akaike's Information Criterion (AIC) were retained and  $R^2$  values were calculated using likelihood ratio tests (lmR2LR, package lmmfit, v. 1.0).

## **Results**

## *Meteorology and soil moisture during the growing season*

Daily mean air temperatures were close to 0 °C at the beginning and the end of the study period, and only reached maximum values of 15 °C (Figure 1a). June-August average temperature was 8.4 °C, cooler than the altitude-corrected climatic value (1962-2007, 9.9 °C). Precipitation (167.5 mm, June-August average) was evenly distributed throughout the study period (Figure 1c), and almost identical to the climatic average (171 mm). Daily radiation input decreased from values of 40-50  $\text{mols m}^{-2} \text{ day}^{-1}$  in June and July to values of *ca.* 20  $\text{mols m}^{-2} \text{ day}^{-1}$  in August and September (Figure 1b). Average soil temperature (measured at a depth of 5 cm) over the growing season was  $9.6 \pm 0.02$  °C, and only forest hummocks (HF) were slightly warmer (0.07 °C,  $P = 0.033$ ) than the overall mean. Soil water content was higher in mire hummocks (HM) compared with forest hummocks (growing season mean  $\pm$  SE values of  $0.67 \pm 0.004 \text{ cm}^3 \text{ cm}^{-3}$  and  $0.19 \pm 0.02 \text{ cm}^3 \text{ cm}^{-3}$ , respectively). Dry hollows (DH) and lichen hummocks (HL) showed similar soil moisture values ( $0.38 \pm 0.002 \text{ cm}^3 \text{ cm}^{-3}$  and  $0.33 \pm 0.002 \text{ cm}^3 \text{ cm}^{-3}$ , respectively) and dynamics throughout the growing season (Figure 1d).

## *Seasonal and diel courses of NEE*

For tundra shrub microsites (i.e. HM, HF and DH), NEE displayed pronounced and very similar seasonal dynamics, whereas the lichen hummocks (HL) showed much lower

fluxes, acting as carbon sources for most of the growing season (Figure 2). Although maximum hourly NEE rates peaked at -12 to -15  $\mu\text{mol CO}_2 \text{ m}^{-2} \text{ s}^{-1}$  around DOY 220 (early August), these values were infrequent and average daytime  $\text{NEE}_{5\%}$  of tundra shrub microsites was -5.2  $\mu\text{mol CO}_2 \text{ m}^{-2} \text{ s}^{-1}$ .  $\text{NEE}_{5\%}$  values for HL plots were very close to zero (-0.09  $\mu\text{mol CO}_2 \text{ m}^{-2} \text{ s}^{-1}$ ). Within tundra shrub microsites,  $\text{NEE}_{5\%}$  did not vary across microsite types ( $P = 0.958$ ). However, a marginally significant difference ( $P = 0.059$ ) was found between night-time  $\text{NEE}_{95\%}$  averaged for all tundra shrub microsites (3.02  $\mu\text{mol CO}_2 \text{ m}^{-2} \text{ s}^{-1}$ ) compared with that of HL plots (1.78  $\mu\text{mol CO}_2 \text{ m}^{-2} \text{ s}^{-1}$ ). The diel courses of NEE confirmed that within-microsite variability was the largest source of variation in NEE fluxes, especially during the peak growing season (Figure 3).

#### *Seasonality in NEE model parameters*

The NEE model performed well (Appendix 2 in Online publication) with better fits for tundra shrub microsites (average adjusted  $R^2 = 0.78$ ) than for HL (average adjusted  $R^2 = 0.53$ ). For all tundra shrub microsites,  $P_{600}$  showed a clear seasonal pattern, with a peak around DOY 220, regardless of the microsite type (Figure 4). Across microsites, quantum efficiency ( $\alpha$ ) tended to show similar increases at the beginning of the growing season. However, the late season decline in  $\alpha$  was not as fast as the early season rise, especially for DH plots, which showed a broad mid-season plateau in the value of  $\alpha$  (Figure 4). HL plots showed much lower values for  $P_{600}$  and  $\alpha$ , representing only 16% and 27%, respectively, of the average values obtained for tundra shrub microsites. Basal respiration also showed peaked dynamics (peak between DOY 195 and 220), although

not as clear as that observed for  $P_{600}$ . One of the HL plots (HL1) had  $R_0$  values of similar magnitude to those of the tundra shrub plots. The  $Q_{10}$  coefficient showed a slightly bimodal pattern, with higher values during early and peak season (Figure 4). Again, higher variability in the parameters of the NEE model was found within microsites compared to that observed among microsites (Figure 4).

#### *NDVI and environmental variables drive NEE seasonality*

The highest NDVI values were observed for HF plots, HL showed the lowest (Figure 4) and HM and DH displayed intermediate NDVI. Although both microsite type ( $F = 12.04$ ,  $d.f. = 8$ ,  $P = 0.0025$ ) and date ( $F = 5.67$ ,  $d.f. = 68$ ,  $P = 0.0201$ ) had an effect on NDVI values, repeating the analysis omitting the HL plots showed that only date remained as a significant effect on NDVI of tundra shrub plots ( $F = 9.20$ ,  $d.f. = 51$ ,  $P = 0.0038$ ) and microsite type played no role ( $F = 2.28$ ,  $df = 6$ ,  $P = 0.1830$ ). Accordingly, the peak value of NDVI showed a tight correlation with both plot vascular biomass and LAI (Figure 5c,d, Table 2). Similarly, maximum NDVI was strongly related to peak  $P_{600}$  and  $R_0$  values (Figure 5a,b, Table 2). However, some discrepancy was observed, as the seasonal course of NDVI showed an early season increase but a very slight late season decline, compared to  $P_{600}$  dynamics (Figure 4).

NDVI and air temperature emerged as the main variables controlling the NEE model parameters for tundra shrub microsites, albeit NDVI was only marginally significant in



the  $R_0$  model (Table 3). A quadratic effect of air temperature and a negative effect of VPD were found for  $P_{600}$ . A negative influence of SWC was observed for  $R_0$  but not for the  $Q_{10}$  coefficient; this latter parameter only varied with DOY (Table 3). No effect of microsite type was observed on  $P_{600}$  or  $\alpha$ , but  $R_0$  did vary across microsites (Table 3). However, this microsite effect was highly correlated with the SWC effects ( $r > 0.97$ ; data not shown).

### *Environmental and structural controls on growing season $CO_2$ fluxes*

Variability in growing season  $CO_2$  fluxes was high within microsite types (Figure 6) and the only consistent differences were found between tundra shrub and lichen microsites (Table 4). Within-microsite variability was less for  $R_{eco}$  than for GPP (Table 4). Lichen-covered plots were a consistent C source whereas tundra shrub plots were C sinks, except for plot HF1 (Figure 6, Table 4). There were large, although only marginally significant, differences in NEE and GPP/LAI between HM and HF microsites, with much higher C uptake per unit leaf area in HM microsites (Table 4). We also found that both LAI and NDVI were good predictors of growing season NEE, GPP and  $R_{eco}$  across plots (Figure 7, Table 2) and that  $R_{eco}$  was strongly related to GPP in a nonlinear fashion (Figure 8, Table 2).

## **Discussion**

Within the studied ecotone, between mire and forest, we observed a great variability in LAI and vascular biomass of tundra shrub and lichen hummocks, characteristic of sub-Arctic areas. NDVI values were tightly related to biomass and LAI across plots, consistent with our hypothesis H1a and with findings for other tundra ecosystems (Boelman and others, 2005; Street and others, 2007). Accordingly, maximum NDVI varied from very low values for HL plots, which were close to pre-growing season, baseline values ( $\approx 0.3$ ) (Huemmrich and others, 2010), to typical maximum NDVI observed in sub-Arctic heath (Street and others, 2007). Seasonal variation of NDVI was also in agreement with that measured in other Arctic ecosystems (La Puma and others, 2007; Huemmrich and others, 2010).

Our results showed slightly lower instantaneous NEE fluxes compared to other studies using automated chambers in northern peatlands (Bubier and others, 2003; Burrows and others, 2005), probably because of lower latitudes and thus milder climatic conditions in these other studies. The length of the sink period was consistent with recent syntheses of eddy flux studies showing that sub-Arctic and Arctic mires display a shorter sink period compared to other boreal peatlands (Lindroth and others, 2007; Lund and others, 2010). We also observed high within-microsite variability in NEE rates, largely related to LAI variations across plots, as has been reported across Arctic tundra sites (Shaver and others, 2007).

## Seasonal drivers of photosynthetic parameters

The parameters describing the response of GPP to light varied seasonally in parallel to NDVI dynamics, and no differences were found amongst the different tundra shrub microsites. Maximum  $P_{600}$  peaked at the end of July and started to decline in August, as observed in other sub-Arctic sites (Alm and others, 1997). Maximum  $P_{600}$  was tightly related with maximum NDVI across plots (H1b), but our mixed-effects models did not include any interaction between vegetation type and DOY (or NDVI) to explain variation in either  $P_{600}$  or  $\alpha$ . Therefore, we could not detect any season-specific differences in the response to light of leaf-area based photosynthesis in our tundra shrub plots, consistent with our hypothesis H2. Similar phenological patterns of leaf area-based  $P_{600}$  have also been reported across *Empetrum* and dry heath patches in sub-Arctic tundra at Abisko, northern Sweden (Street and others, 2007).

Nevertheless, during the late growing season,  $P_{600}$  decreased proportionally faster in comparison to NDVI, concomitant with photoperiod and air temperature decline. This suggests that NDVI may not entirely capture the biochemical downregulation of photosynthesis occurring in late summer. Accordingly, the mixed model results for  $P_{600}$ , apart from the NDVI effects, showed positive, linear and quadratic effects of temperature. A positive influence of air temperature on  $P_{max}$  and on the half-saturation constant of photosynthesis  $k$  (inversely proportional to  $\alpha$ ; cf. Methods), has also been reported for Arctic tundra plots in Alaska (Williams and others, 2006). Moreover, quadratic effects are consistent with nonlinear, delayed responses of  $P_{max}$  to

temperature, as shown previously for two of the species included in this study: *Calluna vulgaris* and *Vaccinium vitis-idaea* (Kulmala and others, 2009, 2011). We have also found a negative effect of VPD on  $P_{600}$  (Williams and others, 2006), which may be due to a combination of two processes: (1) stomatal limitations on  $\text{CO}_2$  assimilation or (2) desiccation-induced reductions in moss photosynthesis. Although we did not find an effect of soil moisture on  $P_{600}$ , as other studies suggest (Kulmala and others, 2011), atmospheric drought alone may induce stomatal closure in some Arctic species (Humphreys and others, 2006). In contrast, gross productivity of mosses appears to be rather insensitive to water content under typical climatic conditions in similar sub-Arctic locations (Street and others, 2012).

#### *Seasonal drivers of respiration parameters*

The seasonal variation in  $R_0$  tracked the dynamics of NDVI and photosynthetic parameters, while the  $Q_{10}$  coefficient decreased slightly throughout the growing season, and did not vary with any environmental variable. These results are in agreement with other chamber-based studies in peatlands (Cai and others, 2010) and the invariant, intrinsic  $Q_{10}$  coefficient for  $R_{eco}$  observed at the global scale (Mahecha and others, 2010). We also observed positive and negative effects of air temperature and soil water content, respectively, on  $R_0$ . If we assume that the NEE model absorbed the response of  $R_{eco}$  to temperature in the  $Q_{10}$  coefficient, we may interpret the apparent positive effect of air temperature as being mediated by recent photosynthesis. High air temperatures are related to increased radiation and both enhance plant photosynthesis, which, in turn,

would boost plant respiration and stimulate respiration of labile exudates by soil microbes, hence increasing  $R_{eco}$ . This explanation would be supported by the tight link between recently assimilated carbon and  $R_{eco}$  observed in temperate heathland (Larsen and others, 2007) and Arctic tundra (Subke and others, 2012). The negative effect of soil water content on  $R_{eco}$  can be explained by low soil aeration limiting microbial decomposition (Johnson and others, 1996), especially in the moister HM microsite, close to the mire edge. Overall, these results support our hypothesis H3b but also highlight additional vegetation controls on  $R_{eco}$ .

#### *Structural controls on growing season $CO_2$ fluxes across microsites*

Importantly, all tundra shrub microsites were consistent  $CO_2$  sinks compared to lichen hummocks, which were  $CO_2$  sources. However, because of the low number of replicates, we could not find significant differences in growing season NEE across microsites. Previous studies have shown that tundra heath patches can be  $CO_2$  sinks (Alm and others, 1997; Marushchak and others, 2013),  $CO_2$  sources (Alm and others, 1999; Heikkinen and others, 2004) or  $CO_2$  neutral (Nobrega & Grogan, 2008; Maanavilja and others, 2011), probably reflecting differences in LAI and specific environmental conditions. Likewise, bare peat and lichen communities are consistent  $CO_2$  sources (Heikkinen and others, 2004; Marushchak and others, 2013).

Across plots, all growing season  $CO_2$  fluxes were strongly and positively related to LAI,

as also recently observed in a reconstruction of seasonal CO<sub>2</sub> budget using manual chamber measurements (Marushchak and others, 2013). Similarly, we observed a good correspondence between peak NDVI and all the CO<sub>2</sub> flux components integrated over the growing season. While the link between NDVI and GPP is mechanistically straightforward, the association between NDVI and  $R_{eco}$  might be explained by a high contribution of autotrophic respiration to  $R_{eco}$  and/or a tight link between growing season  $R_{eco}$  and GPP, as we observed here. NDVI has indeed been related to instantaneous or daily GPP and  $R_{eco}$  (McMichael, 1999; Boelman and others, 2003), although sometimes with a low explanatory power (La Puma and others, 2007; Dagg & Lafleur, 2010).

Although the relationship between NDVI and NEE was weaker than for GPP and  $R_{eco}$ , NDVI still explained a high proportion of NEE variation, in contrast with the weak or non-existent relationships reported for other plot-scale studies in the Arctic (La Puma and others, 2007; Dagg & Lafleur, 2010). Our results are thus in agreement with the observed control of LAI on ecosystem-level NEE across northern peatlands and tundra sites (Lund and others, 2010). We are not aware of any other study in low Arctic ecosystems showing these strong vegetation controls on growing season NEE and its components for patch-scale CO<sub>2</sub> fluxes, measured at high temporal resolution over the course of an entire growing season.

*Implications for CO<sub>2</sub> flux upscaling*

The NEE model employed in this paper does not include LAI as an input, as the one proposed by Shaver and others (2007) does. Hence, here, seasonal variation in the parameters of the NEE model implicitly includes seasonal LAI dynamics and we analyse a posteriori the roles of structural vs. environmental drivers in controlling NEE using a mixed-effects model. We follow this approach because one of the aims of this paper is to test whether our data support the reported functional convergence in NEE controls across Arctic ecosystems, not to test the direct applicability of the model by Shaver and others in our site. Moreover, there are some drawbacks to the application of this model, such as the uncertainty in LAI estimation (cf. discussion in Shaver and others 2007).

Overall, our results are broadly consistent with this functional convergence, but underline the additional role of air temperature and VPD effects on the seasonal light response of tundra vegetation. In addition, GPP per unit leaf area in mire hummocks (HM) was more than double the value observed for drier forest hummocks (HF), and similar to dry hollows (DH). The similarity in GPP/LAI observed between DH and HM microsites (i.e. under contrasting soil moisture conditions) would not support a hypothetical effect of soil moisture in reducing GPP/LAI, although the HF microsite was even drier than the DH microsite and, therefore, a drought effect could not be discarded. Various studies on Arctic tundra have indeed shown increased productivity in wetter patches (Nobrega & Grogan, 2008; Dagg & Lafleur, 2011) and reduced light use efficiency in dry microsites (Huemmrich and others, 2010). However, a reduction in GPP/LAI could be attributed to a suboptimal arrangement of vegetation within the transition zone. A recent study has reported this phenomenon for ecotones containing *E. nigrum* in another sub-Arctic site and *Betula nana*-dominated transects within the same

study area (Fletcher and others, 2012). However, whether this is the only explanation for the observed differences is doubtful, as changes in vegetation composition between HF and HM plots are minor (Table 1). Our results thus only partly support hypothesis H4 and suggest, for growing season CO<sub>2</sub> fluxes, a decrease in GPP/LAI within sub-Arctic ecotones from mires to forest, which may be mediated by reductions in soil moisture.

Another important implication of our results concerns the consistent CO<sub>2</sub> sources observed in lichen hummocks. The analysis of a land classification map obtained from airborne photography (T. Hill, unpublished) shows that *ca.* 20% of the area in the ecotone between forest and mire is covered by lichen. Therefore, these hotspots for C release will significantly contribute to reduce the C sink capacity at the landscape scale. However, poorly vegetated and bare peat hummocks usually present frozen cores (Van Vliet-Lanoe & Seppala, 2002), as observed at the study site (Wayolle, 2011), which may degrade with climate warming and result in increased net C uptake after shrub colonisation of these hummocks (Bosiö and others, 2012).

#### *Concluding remarks*

Our results showed a great variability in NEE fluxes within tundra shrub and lichen microsites at diel and seasonal timescales, which could be largely explained by microclimate and LAI. Given the good correspondence observed between vegetation



parameters and NDVI, this spectral index was found to be a good predictor of both maximum photosynthetic and respiratory potential. Other studies on low-stature vegetation have shown that broad-band NDVI can be used to predict NEE light response parameters (Wohlfahrt and others, 2010). Nevertheless, we have also found that other environmental drivers modulate the dynamics of vegetation controls on CO<sub>2</sub> fluxes, and they should therefore be included in models of NEE in low Arctic ecosystems (Lorantý and others, 2011). We have also shown that NDVI can successfully predict growing season GPP,  $R_{eco}$  and NEE of sub-Arctic heath and lichen communities. Finally, the comparatively low GPP/LAI observed in hummocks near the forest edge is consistent with a decreased productivity observed in transition zones between Arctic vegetation types and soil moisture constraints on plant assimilation.

## Acknowledgements

Thanks to all the staff at the Kevo Subarctic Research Institute and to all the colleagues who collaborated in lab and fieldwork tasks, especially D. Sayer, T. August, K. Leslie and A. Robertson. Thanks to B. Fletcher, V. Sloan and G. Phoenix for their plant survey data and to T. Hill for the land classification map. We are grateful to P. Stoy and M. Williams for helpful comments on earlier versions of the manuscript and also to E. Rastetter for his feedback. This study was funded by NERC (UK) through the ABACUS consortium (Arctic Biosphere-Atmosphere Coupling at Multiple Scales, [www.geos.ed.ac.uk/abacus](http://www.geos.ed.ac.uk/abacus); grant No. NE/D005760/1), within the framework of the International Polar Year (2007-2008). RP also benefited from a contract within the

MONTES project (CSD 2008-00040) and a ‘Juan de la Cierva’ fellowship, both funded by the Spanish Ministry of Science and Innovation.

## References

Alm J, Schulman L, Walden J, Nykänen H, Martikainen PJ, Silvola J. 1999. Carbon balance of a boreal bog during a year with an exceptionally dry summer. *Ecology* 80: 161–174.

Alm J, Talanov A, Saarnio S, Silvola J, Ikkonen E, Aaltonen H, Nykänen H, Martikainen PJ. 1997. Reconstruction of the carbon balance for microsites in a boreal oligotrophic pine fen, Finland. *Oecologia* 110: 423–431.

Asner GP, Scurlock JMO, A. Hicke J. 2003. Global synthesis of leaf area index observations: implications for ecological and remote sensing studies. *Global Ecology and Biogeography* 12: 191–205.

Atkin OK, Bruhn D, Tjoelker MG. 2005. Response of Plant Respiration to Changes in Temperature: Mechanisms and Consequences of Variations in  $Q_{10}$  Values and Acclimation. In: Lambers H, Ribas-Carbó M, eds. *Advances in Photosynthesis and Respiration. Plant Respiration: From Cell to Ecosystem*. Dordrecht, The Netherlands: Springer, 95–135.

Beck PSA, Juday GP, Alix C, Barber VA, Winslow SE, Sousa EE, Heiser P, Herriges JD, Goetz SJ. 2011. Changes in forest productivity across Alaska consistent with biome shift. *Ecology Letters* 14:373–379.

595 Boelman NT, Stieglitz M, Griffin KL, Shaver GR. 2005. Inter-annual variability of  
 596 NDVI in response to long-term warming and fertilization in wet sedge and tussock  
 597 tundra. *Oecologia* 143: 588–597.

598 Boelman NT, Stieglitz M, Rueth HM, Sommerkorn M, Griffin KL, Shaver GR, Gamon  
 599 JA. 2003. Response of NDVI, biomass, and ecosystem gas exchange to long-term  
 600 warming and fertilization in wet sedge tundra. *Oecologia* 135: 414–421.

601 Bosiö J, Johansson M, Callaghan T, Johansen B, Christensen T. 2012. Future vegetation  
 602 changes in thawing subarctic mires and implications for greenhouse gas exchange—a  
 603 regional assessment. *Climatic Change*: 1–20.

604 Bubier J, Crill P, Mosedale A, Frohking S, Linder E. 2003. Peatland responses to  
 605 varying interannual moisture conditions as measured by automatic CO<sub>2</sub> chambers.  
 606 *Global Biogeochemical Cycles* 17: 1066.

607 Burrows EH, Bubier JL, Mosedale A, Cobb GW, Crill PM. 2005. Net Ecosystem  
 608 Exchange of Carbon dioxide in a Temperate Poor Fen: a Comparison of Automated and  
 609 Manual Chamber Techniques. *Biogeochemistry* 76: 21–45.

610 Cai T, Flanagan LB, Syed KH. 2010. Warmer and drier conditions stimulate respiration  
 611 more than photosynthesis in a boreal peatland ecosystem: Analysis of automatic  
 612 chambers and eddy covariance measurements. *Plant, Cell & Environment* 33: 394–407.

613 Christensen JH, Hewitson B, Busuioc A, Chen A, Gao X, Held I, Jones R, Kolli RK,  
 614 Kwon WT, Laprise R. 2007. Regional climate projections. In: Solomon S, Qin D,  
 615 Manning M, Chen Z, Marquis M, Averyt KB, Tignor M, Miller HL, eds. *Climate*  
 616 *Change 2007: The Physical Science Basis. Contribution of Working Group I to the*

617 Fourth Assessment Report of the Intergovernmental Panel on Climate Change.  
 618 Cambridge, UK and New York, USA: Cambridge University Press, p847–940.

619 Dagg J, Lafleur P. 2010. An application of plot-scale NDVI in predicting carbon  
 620 dioxide exchange and leaf area index in heterogeneous subarctic tundra. *Canadian*  
 621 *Journal of Remote Sensing* 36: S111–S123.

622 Dagg J, Lafleur P. 2011. Vegetation Community, Foliar Nitrogen, and Temperature  
 623 Effects on Tundra CO<sub>2</sub> Exchange across a Soil Moisture Gradient. *Arctic, Antarctic,*  
 624 *and Alpine Research* 43: 189–197.

625 Dorrepaal E, Toet S, Van Logtestijn RSP, Swart E, Van de Weg MJ, Callaghan TV,  
 626 Aerts R. 2009. Carbon respiration from subsurface peat accelerated by climate warming  
 627 in the subarctic. *Nature* 460: 616–619.

628 Elmendorf SC, Henry GHR, Hollister RD, Björk RG, Boulanger-Lapointe N, Cooper  
 629 EJ, Cornelissen JHC, Day TA, Dorrepaal E, Elumeeva TG, Gill M, Gould WA, Harte J,  
 630 Hik DS, Hofgaard A, Johnson DR, Johnstone JF, Jónsdóttir IS, Jorgenson JC,  
 631 Klanderud K, Klein JA, Koh S, Kudo G, Lara M, Lévesque E, Magnússon B, May JL,  
 632 Mercado-Díaz JA, Michelsen A, Molau U, Myers-Smith IH, Oberbauer SF, Onipchenko  
 633 VG, Rixen C, Schmidt NM, Shaver GR, Spasojevic MJ, Þórhallsdóttir ÞE, Tolvanen A,  
 634 Troxler T, Tweedie CE, Villareal S, Wahren C-H, Walker X, Webber PJ, Welker JM,  
 635 Wipf S. 2012. Plot-scale evidence of tundra vegetation change and links to recent  
 636 summer warming. *Nature Climate Change* 2: 453–457.

637 Fletcher BJ, Gornall JL, Poyatos R, Press MC, Stoy PC, Huntley B, Baxter R, Phoenix  
 638 GK. 2012. Photosynthesis and productivity in heterogeneous arctic tundra:

639 consequences for ecosystem function of mixing vegetation types at stand edges. *Journal*  
 640 *of Ecology* 100: 441–451.

641 Heikkinen JEP, Virtanen T, Huttunen JT, Elsakov V, Martikainen PJ, others. 2004.  
 642 Carbon balance in East European tundra. *Global Biogeochemical Cycles* 18: 1–14.

643 Heinemeyer A, Di Bene C, Lloyd AR, Tortorella D, Baxter R, Huntley B, Gelsomino A,  
 644 Ineson P. 2011. Soil respiration: implications of the plant-soil continuum and respiration  
 645 chamber collar-insertion depth on measurement and modelling of soil CO<sub>2</sub> efflux rates  
 646 in three ecosystems. *European Journal of Soil Science* 62: 82–94.

647 Huemmrich K., Gamon JA, Tweedie CE, Oberbauer SF, Kinoshita G, Houston S,  
 648 Kuchy A, Hollister RD, Kwon H, Mano M. 2010. Remote sensing of tundra gross  
 649 ecosystem productivity and light use efficiency under varying temperature and moisture  
 650 conditions. *Remote Sensing of Environment* 114: 481–489.

651 Humphreys ER, Lafleur PM, Flanagan LB, Hedstrom N, Syed KH, Glenn AJ, Granger  
 652 R. 2006. Summer carbon dioxide and water vapor fluxes across a range of northern  
 653 peatlands. *Journal of Geophysical Research* 111: G04011.

654 Johnson LC, Shaver GR, Giblin AE, Nadelhoffer KJ, Rastetter ER, Laundre JA, Murray  
 655 GL. 1996. Effects of drainage and temperature on carbon balance of tussock tundra  
 656 microcosms. *Oecologia* 108: 737–748.

657 Jones HG. 1992. *Plants and microclimate: a quantitative approach to environmental*  
 658 *plant physiology*. Cambridge, UK.: Cambridge University Press. 428p.

659 Kulmala L, Pumpanen J, Hari P, Vesala T. 2011. Photosynthesis of ground vegetation  
660 in different aged pine forests: Effect of environmental factors predicted with a process-  
661 based model. *Journal of Vegetation Science* 22: 96–110.

662 Kulmala L, Pumpanen J, Vesala T, Hari P. 2009. Photosynthesis of boreal ground  
663 vegetation after a forest clear-cut. *Biogeosciences* 6: 2495–2507.

664 Kutzbach L, Schneider J, Sachs T, Giebels M, Nykanen H, Shurpali NJ, Martikainen PJ,  
665 Alm J, Wilmking M. 2007. CO<sub>2</sub> flux determination by closed-chamber methods can be  
666 seriously biased by inappropriate application of linear regression. *Biogeosciences* 4:  
667 1005–1025.

668 Larsen KS, Ibrom A, Beier C, Jonasson S, Michelsen A. 2007. Ecosystem respiration  
669 depends strongly on photosynthesis in a temperate heath. *Biogeochemistry* 85: 201–  
670 213.

671 Limpens J, Berendse F, Blodau C, Canadell JG, Freeman C, Holden J, Roulet N, Rydin  
672 H, Schaepman-Strub G. 2008. Peatlands and the carbon cycle: from local processes to  
673 global implications: a synthesis. *Biogeosciences* 5: 1475.

674 Lindroth A, Lund M, Nilsson M, Aurela M, Christensen TR, Laurila T, Rinne J, Riutta  
675 T, Sagerfors J, Ström L. 2007. Environmental controls on the CO<sub>2</sub> exchange in north  
676 European mires. *Tellus B* 59: 812–825.

677 Loranty MM, Goetz SJ, Rastetter EB, Rocha AV, Shaver GR, Humphreys ER, Lafleur  
678 PM. 2011. Scaling an Instantaneous Model of Tundra NEE to the Arctic Landscape.  
679 *Ecosystems* 14: 76–93.

680 Lund M, Lafleur PM, Roulet NT, Lindroth A, Christensen TR, Aurela M, Chojnicki  
 681 BH, Flanagan LB, Humphreys ER, Laurila T. 2010. Variability in exchange of CO<sub>2</sub>  
 682 across 12 northern peatland and tundra sites. *Global Change Biology* 16: 2436–2448.

683 Maanavilja L, Riutta T, Aurela M, Pulkkinen M, Laurila T, Tuittila E-S. 2011. Spatial  
 684 variation in CO<sub>2</sub> exchange at a northern aapa mire. *Biogeochemistry* 104: 325–345.

685 Mahecha MD, Reichstein M, Carvalhais N, Lasslop G, Lange H, Seneviratne SI, Vargas  
 686 R, Ammann C, Arain MA, Cescatti A, Janssens IA, Migliavacca M, Montagnani L  
 687 Richardson, AD. 2010. Global Convergence in the Temperature Sensitivity of  
 688 Respiration at Ecosystem Level. *Science* 329: 838–840.

689 Marushchak ME, Kiepe I, Biasi C, Elsakov V, Friborg T, Johansson T, Soegaard H,  
 690 Virtanen T, Martikainen PJ. 2013. Carbon dioxide balance of subarctic tundra from plot  
 691 to regional scales. *Biogeosciences* 10: 437–452.

692 McMichael CE. 1999. Estimating CO<sub>2</sub> exchange at two sites in Arctic tundra  
 693 ecosystems during the growing season using a spectral vegetation index. *International*  
 694 *Journal of Remote Sensing* 20: 683–698.

695 Moore TR, Bubier JL, Frolking SE, Lafleur PM, Roulet NT. 2002. Plant biomass and  
 696 production and CO<sub>2</sub> exchange in an ombrotrophic bog. *Journal of Ecology* 90: 25–36.

697 Natali SM, Schuur EAG, Rubin RL. 2012. Increased plant productivity in Alaskan  
 698 tundra as a result of experimental warming of soil and permafrost. *Journal of Ecology*  
 699 100: 488–498.

700 Nobrega S, Grogan P. 2008. Landscape and Ecosystem-Level Controls on Net Carbon  
 701 Dioxide Exchange along a Natural Moisture Gradient in Canadian Low Arctic Tundra.  
 702 *Ecosystems* 11: 377–396.

703 Oberbauer SF, Tweedie CE, Welker JM, Fahnestock JT, Henry GHR, Webber PJ,  
 704 Hollister RD, Walker MD, Kuchy A, Elmore E. 2007. Tundra CO<sub>2</sub> fluxes in response to  
 705 experimental warming across latitudinal and moisture gradients. *Ecological*  
 706 *Monographs* 77: 221–238.

707 Oechel WC, Vourlitis GL, Brooks S, Crawford TL, Dumas E. 1998. Intercomparison  
 708 among chamber, tower, and aircraft net CO<sub>2</sub> and energy fluxes measured during the  
 709 Arctic System Science Land-Atmosphere-Ice Interactions (ARCSS-LAII) Flux Study.  
 710 *Journal of Geophysical Research-Atmospheres* 103: 28993–29003.

711 Pelletier L, Garneau M, Moore T. 2011. Variation in CO<sub>2</sub> exchange over three summers  
 712 at microform scale in a boreal bog, Eastmain region, Québec, Canada. *Journal of*  
 713 *Geophysical Research-Biogeosciences* 116: G03019.

714 Pinheiro JC, Bates DM. 2000. Mixed-effects models in S and S-PLUS. Springer Verlag.  
 715 528p.

716 La Puma IP, Philippi TE, Oberbauer SF. 2007. Relating NDVI to ecosystem CO<sub>2</sub>  
 717 exchange patterns in response to season length and soil warming manipulations in arctic  
 718 Alaska. *Remote Sensing of Environment* 109: 225–236.

719 R Development Core Team. 2009. R: A Language and Environment for Statistical  
 720 Computing. R Foundation for Statistical Computing, Vienna, Austria.



Riutta T, Laine J, Aurela M, Rinne J, Vesala T, Laurila T, Haapanala S, Pihlatie M,  
 Tuittila E-S. 2007. Spatial variation in plant community functions regulates carbon gas  
 dynamics in a boreal fen ecosystem. *Tellus B* 59: 838–852.

Schuur EAG, Vogel JG, Crummer KG, Lee H, Sickman JO, Osterkamp TE. 2009. The  
 effect of permafrost thaw on old carbon release and net carbon exchange from tundra.  
*Nature* 459: 556–559.

Shaver GR, Street LE, Rastetter EB, Van Wijk MT, Williams M. 2007. Functional  
 convergence in regulation of net CO<sub>2</sub> flux in heterogeneous tundra landscapes in Alaska  
 and Sweden. *Journal of Ecology* 95: 802–817.

Soegaard H, Nordstroem C, Friberg T, Hansen BU, Christensen TR, Bay C. 2000.  
 Trace gas exchange in a high-Arctic valley: 3. Integrating and scaling CO<sub>2</sub> fluxes from  
 canopy to landscape using flux data, footprint modeling, and remote sensing. *Global  
 Biogeochemical Cycles* 14: 725–744.

Spadavecchia L, Williams M, Bell R, Stoy PC, Huntley B, Van Wijk MT. 2008.  
 Topographic controls on the leaf area index and plant functional type of a tundra  
 ecosystem. *Journal of Ecology* 96: 1238–1251.

Stoy PC, Williams M, Evans JG, Prieto-Blanco A, Disney M, Hill TC, Wade TJ, Street  
 LE. Upscaling tundra CO<sub>2</sub> exchange from chamber to eddy covariance tower. *Arctic,  
 Antarctic, and Alpine Research* 45: 275–284.

Street LE, Shaver GR, Williams M, Van Wijk MT. 2007. What is the relationship  
 between changes in canopy leaf area and changes in photosynthetic CO<sub>2</sub> flux in arctic  
 ecosystems? *Journal of Ecology* 95: 139–150.

743 Street LE, Stoy PC, Sommerkorn M, Fletcher BJ, Sloan VL, Hill TC, Williams M.  
 744 2012. Seasonal bryophyte productivity in the sub-Arctic: a comparison with vascular  
 745 plants. *Functional Ecology* 26: 365–378.

746 Subke J-A, Heinemeyer A, Vallack H, Leronni V, Baxter R, Ineson P. 2012. Fast  
 747 assimilate turnover revealed by in situ  $^{13}\text{CO}_2$  pulse-labelling in Subarctic tundra. *Polar*  
 748 *Biology* 35: 1209–1219.

749 Turunen J, Tomppo E, Tolonen K, Reinikainen A. 2002. Estimating carbon  
 750 accumulation rates of undrained mires in Finland – application to boreal and subarctic  
 751 regions. *The Holocene* 12: 69–80.

752 Van Vliet-Lanoe B, Seppala M. 2002. Stratigraphy, age and formation of peaty earth  
 753 hummocks (pounus), Finnish Lapland. *The Holocene* 12: 187–199.

754 Wayolle AAJ. 2011. Multiscale Soil Carbon Distribution in Two Sub-Arctic  
 755 Landscapes. PhD dissertation, University of Stirling, Stirling, UK.

756 Van Wijk MT, Williams M, Shaver GR. 2005. Tight coupling between leaf area index  
 757 and foliage N content in arctic plant communities. *Oecologia* 142: 421–427.

758 Williams M, Street LE, Wijk MT, Shaver GR. 2006. Identifying Differences in Carbon  
 759 Exchange among Arctic Ecosystem Types. *Ecosystems* 9: 288–304.

760 Wohlfahrt G, Pilloni S, Hörtnagl L, Hammerle A. 2010. Estimating carbon dioxide  
 761 fluxes from temperate mountain grasslands using broad-band vegetation indices.  
 762 *Biogeosciences* 7: 683–694.

763

## Table legends

Table 1. Vegetation characteristics of the study plots: percent cover of the dominant species, total percent cover of vascular species, biomass and leaf area index (LAI) of vascular plants and maximum patch-scale normalised differential vegetation index (NDVI).

Table 2. Summary statistics for the relationships among NEE model parameters, vegetation parameters and cumulative CO<sub>2</sub> fluxes, depicted in Figures 5, 7 and 8.

Table 3. Statistics for mixed models of NEE model parameters as a function of environmental and vegetation variables. The response variable was log-transformed when needed. Vegetation type HM has been considered the reference level. Rows in bold show statistically significant effects ( $P < 0.05$ ) and underlined results depict marginally significant effects ( $0.1 < P < 0.05$ ).

Table 4. Growing season cumulative values of CO<sub>2</sub>-C fluxes per ground area (g C m<sup>-2</sup>) and expressed per unit leaf area for the studied vegetation types. Different letters indicate significant ( $P < 0.05$ ) differences among types. Marginal differences ( $0.1 < P < 0.05$ ) between two vegetation types are also underlined.

Table 1.

Plot	Vegetation Type	Species	Vascular % cover	Non-vascular % cover	Vascular Biomass (g m <sup>-2</sup> )	Vascular LAI m <sup>2</sup> m <sup>-2</sup>	NDVI <sub>max</sub>
HM1	Mire hummock	<i>Empetrum nigrum</i> (25) <i>Rubus chamaemorus</i> (6) <i>Sphagnum</i> spp. (11)	41	11	82.9	0.37	0.65
HM2	Mire hummock	<i>Empetrum nigrum</i> (48) <i>Vaccinium uliginosum</i> (3)	53	5	228.7	0.94	0.72
HM3	Mire hummock	<i>Empetrum nigrum</i> (31) <i>Vaccinium vitis-idaea</i> (11) <i>Pleurozium schreberi</i> (12)	52	15	42.6	0.27	0.69
HF1	Forest hummock	<i>Empetrum nigrum</i> (24) <i>Vaccinium vitis-idaea</i> (21) <i>Sphagnum</i> spp. (11)	49	23	107.9	0.63	0.69
HF2	Forest hummock	<i>Empetrum nigrum</i> (38) <i>Vaccinium vitis-idaea</i> (14)	52	7	248.8	1.22	0.78
HF3	Forest hummock	<i>Empetrum nigrum</i> (51) <i>Vaccinium myrtillus</i> (14) Lichen (10)	75	10	393.9	2.07	0.85
HL1	Eroded hummock	Lichen (17)	0	17	0	0	0.46
HL2	Eroded hummock	Lichen (15) Acrocarpous moss (28)	0	43	0	0	0.41
HL3	Eroded hummock	Lichen (25) Acrocarpous moss (17)	5	44	0	0	0.41
DH1	Dry hollow	<i>Calluna vulgaris</i> (40) <i>Vaccinium uliginosum</i> (10)	52	13	295.5	0.85	0.79
DH2	Dry hollow	<i>Calluna vulgaris</i> (20)	26	8	62.8	0.18	0.65

DH3	Dry hollow	<i>Vaccinium myrtillus</i> (3)					
		<i>Calluna vulgaris</i> (51)	58	3	144.0	0.40	0.67
		<i>Vaccinium uliginosum</i> (2)					

---

Table 2.

Response variable	Explanatory variable	Intercept	Slope	$R^2$
<i>NEE model parameters</i>				
$\ln(\text{Maximum } P_{600})$	$\ln(\text{Maximum NDVI})$	$3.56 \pm 0.14$	$3.06 \pm 0.27$	0.92
$\ln(\text{Maximum } R_0)$	$\ln(\text{Maximum NDVI})$	$1.83 \pm 0.16$	$1.69 \pm 0.31$	0.73
<i>Vegetation parameters</i>				
Vascular biomass	Maximum NDVI	$-10003.4 \pm 164.1$	$1638.2 \pm 226.5$	0.87
Vascular LAI	Maximum NDVI	$-5.00 \pm 0.92$	$8.00 \pm 1.27$	0.83
<i>Cumulative CO<sub>2</sub> fluxes</i>				
NEE	Maximum NDVI	$316.8 \pm 86.48$	$-564.73 \pm 130.46$	0.62
$\ln(-\text{GPP})$	$\ln(\text{Maximum NDVI})$	$6.81 \pm 0.11$	$3.12 \pm 0.22$	0.95
$R_{eco}$	Maximum NDVI	$-56.29 \pm 44.71$	$427.80 \pm 67.44$	0.78
NEE	LAI	$-20.80 \pm 40.00$	$-87.18 \pm 41.94$	0.29
GPP	LAI	$-241.03 \pm 37.92$	$-126.72 \pm 39.76$	0.53
$\log(R_{eco})$	$\ln(\text{LAI})$	$5.61 \pm 0.05$	$0.17 \pm 0.06$	0.51
$\ln(R_{eco})$	$\ln(-\text{GPP})$	$3.00 \pm 0.39$	$0.44 \pm 0.07$	0.76

Table 3.

Response variable	Fixed effect	Estimate	SE	df	t	P-value	AIC	R <sup>2</sup>
log( $P_{600}$ )	<b>(Intercept)</b>	<b>-1.446</b>	<b>0.402</b>	<b>218</b>	<b>-3.594</b>	<b>0.0004</b>	124.29	0.88
	<b>NDVI</b>	<b>1.522</b>	<b>0.387</b>	<b>218</b>	<b>3.932</b>	<b>0.0001</b>		
	<b><math>T_0</math></b>	<b>0.199</b>	<b>0.029</b>	<b>218</b>	<b>6.885</b>	<b>0.0000</b>		
	<b><math>T_0^2</math></b>	<b>-0.005</b>	<b>0.001</b>	<b>218</b>	<b>-3.954</b>	<b>0.0001</b>		
	<b>VPD</b>	<b>-0.510</b>	<b>0.223</b>	<b>218</b>	<b>-2.287</b>	<b>0.0232</b>		
	Vegtype: HF	-0.216	0.221	8	-0.977	0.3571		
	Vegtype: DH	-0.137	0.216	8	-0.636	0.5425		
	Vegtype: HL	-1.442	0.231	8	-6.234	0.0002		
	<b>DOY</b>	<b>0.007</b>	<b>0.001</b>	<b>218</b>	<b>5.262</b>	<b>0.0000</b>		
log( $\alpha$ )	<b>(Intercept)</b>	<b>-0.069</b>	<b>0.014</b>	<b>235</b>	<b>-4.909</b>	<b>0.0000</b>	-1261.98	0.41
	<b>NDVI</b>	<b>0.066</b>	<b>0.013</b>	<b>235</b>	<b>5.048</b>	<b>0.0000</b>		
	<b><math>T_0</math></b>	<b>0.002</b>	<b>0.000</b>	<b>235</b>	<b>5.092</b>	<b>0.0000</b>		
	<b>DOY</b>	<b>0.000</b>	<b>0.000</b>	<b>235</b>	<b>4.232</b>	<b>0.0000</b>		
log( $R_0$ )	<b>(Intercept)</b>	<b>3.211</b>	<b>1.250</b>	<b>220</b>	<b>2.569</b>	<b>0.0109</b>	359.05	0.50
	<u>NDVI</u>	<u>0.904</u>	<u>0.511</u>	<u>220</u>	<u>1.769</u>	<u>0.0782</u>		
	<b>Vegtype: HF</b>	<b>-2.566</b>	<b>0.803</b>	<b>8</b>	<b>-3.195</b>	<b>0.0127</b>		
	<b>Vegtype: DH</b>	<b>-1.726</b>	<b>0.533</b>	<b>8</b>	<b>-3.238</b>	<b>0.0119</b>		
	<b>Vegtype: HL</b>	<b>-2.567</b>	<b>0.625</b>	<b>8</b>	<b>-4.109</b>	<b>0.0034</b>		
	<b><math>T_0</math></b>	<b>0.036</b>	<b>0.009</b>	<b>220</b>	<b>4.066</b>	<b>0.0001</b>		
	<b>SWC</b>	<b>-5.667</b>	<b>1.617</b>	<b>220</b>	<b>-3.505</b>	<b>0.0006</b>		
$Q_{10}$	<b>(Intercept)</b>	<b>2.880</b>	<b>0.421</b>	<b>237</b>	<b>6.849</b>	<b>0.0000</b>	650.19	0.03
	<b>DOY</b>	<b>-0.006</b>	<b>0.002</b>	<b>237</b>	<b>-2.911</b>	<b>0.0039</b>		

Table 4.

	Vegetation Type			
	HM	HF	DH	HL
NEE	-92.7±10.6 <sup>a</sup>	-82.3±86.1 <sup>a</sup>	-84.6±40.2 <sup>a</sup>	66.1±23.8 <sup>a</sup>
GPP	-331.1±14.7 <sup>a</sup>	-369.3±80.1 <sup>a</sup>	-312.3±73.2 <sup>a</sup>	-61.1±4.9 <sup>b</sup>
$R_{eco}$	239.6±6.1 <sup>a</sup>	287.2±12.2 <sup>a</sup>	<u>227.4±33.2<sup>ab</sup></u>	<u>126.1±26.4<sup>b</sup></u>
NEE/LAI	<u>-246.7±97.6<sup>a</sup></u>	<u>-28.12±57.8<sup>a</sup></u>	-162.7±35.2 <sup>a</sup>	na
GPP/LAI	<u>-833.5±279.9<sup>a</sup></u>	<u>-307.6±38.1<sup>a</sup></u>	-778.4±149.8 <sup>a</sup>	na
$R_{eco}$ /LAI	594.5±186.9 <sup>a</sup>	280.1±95.5 <sup>a</sup>	175.4±95.5 <sup>a</sup>	na



## Figure legends

Figure 1. Seasonal course of daily aggregates of environmental variables: a) mean site air temperature b) Photosynthetically Active Radiation (PAR), c) precipitation and d) volumetric soil content (0-10 cm) measured in a representative plot of each vegetation type. Panel a) also shows hourly variation in air temperature in grey.

Figure 2. Time series of hourly Net Ecosystem CO<sub>2</sub> Exchange (NEE) measured in three replicated chambers in a) mire hummocks (HM), b) forest hummocks (HF), c) dry hollows (DH) and d) lichen-covered hummocks (HL).

Figure 3. Diel courses of NEE during the growing season: DOY 170, DOY 195, DOY 220 and DOY 254. Lines depict hourly NEE for three replicated chambers in mire hummocks (HM, 1st row), forest hummocks (HF, 2nd row), dry hollows (DH, 3<sup>rd</sup> row) and lichen-covered hummocks (HL, 4<sup>th</sup> row).

Figure 4. Seasonal course of NEE model parameters for all measured chambers, according to vegetation type: mire hummocks (HM, 1st column), forest hummocks (HF, 2nd column), dry hollows (DH, 3<sup>rd</sup> column) and lichen-covered hummocks (HL, 4<sup>th</sup> column).

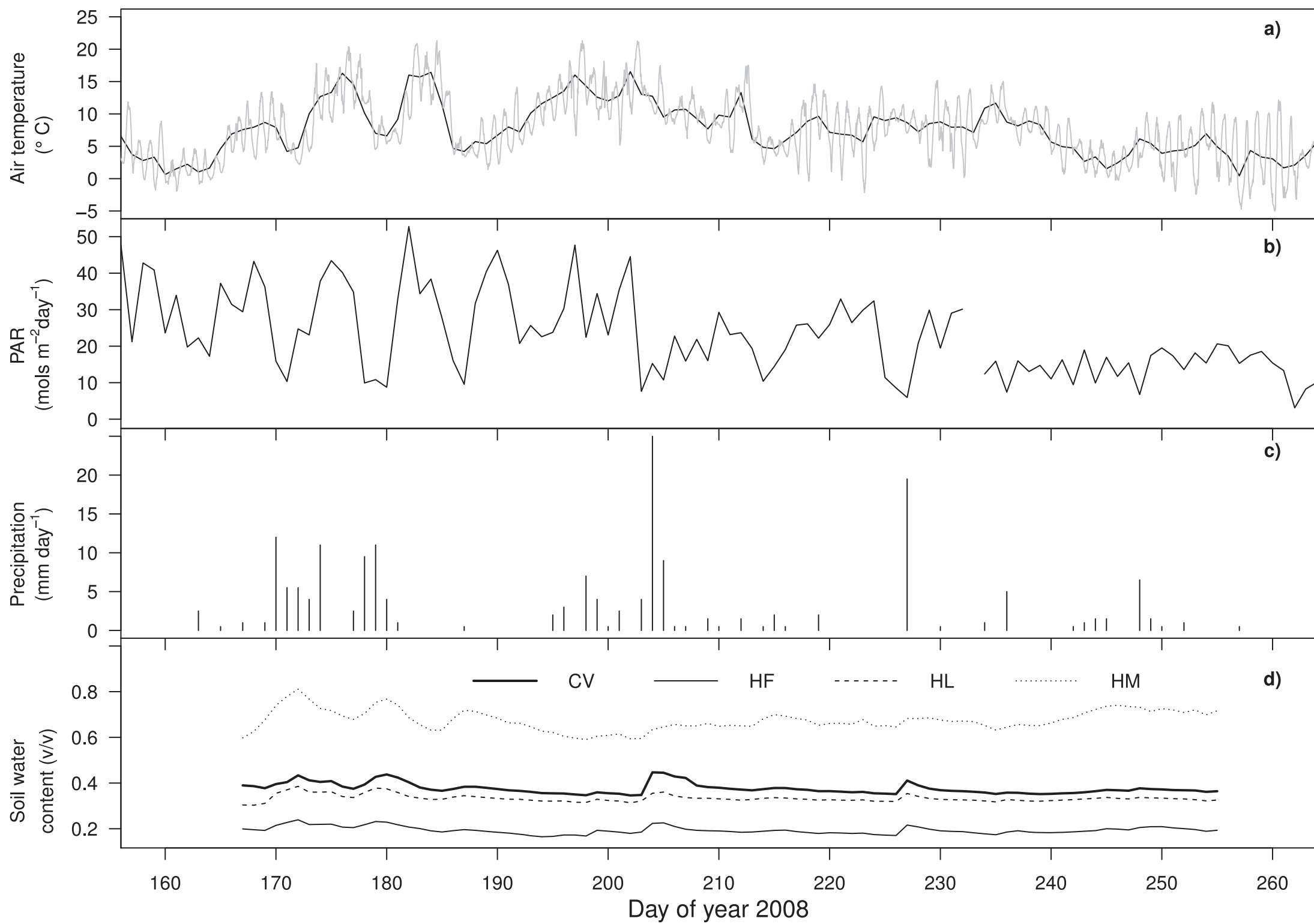
Figure 5. Relationships between maximum NDVI and: maximum values of (a)  $P_{600}$  and (b)  $R_o$ , (c) plot vascular biomass and (d) plot LAI.

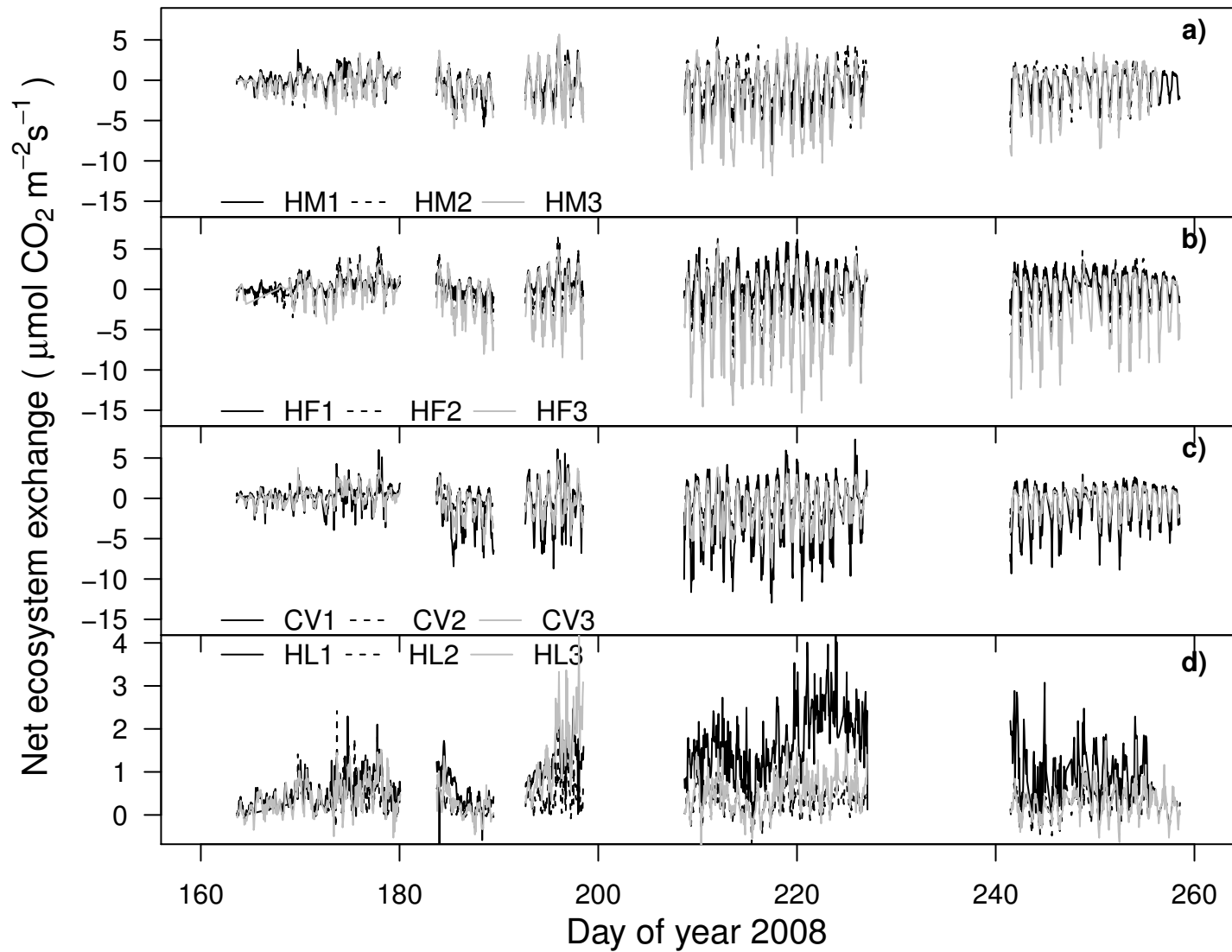
Figure 6. Growing season cumulative NEE (a), GPP (b) and  $R_{eco}$  (c) for all measured plots.

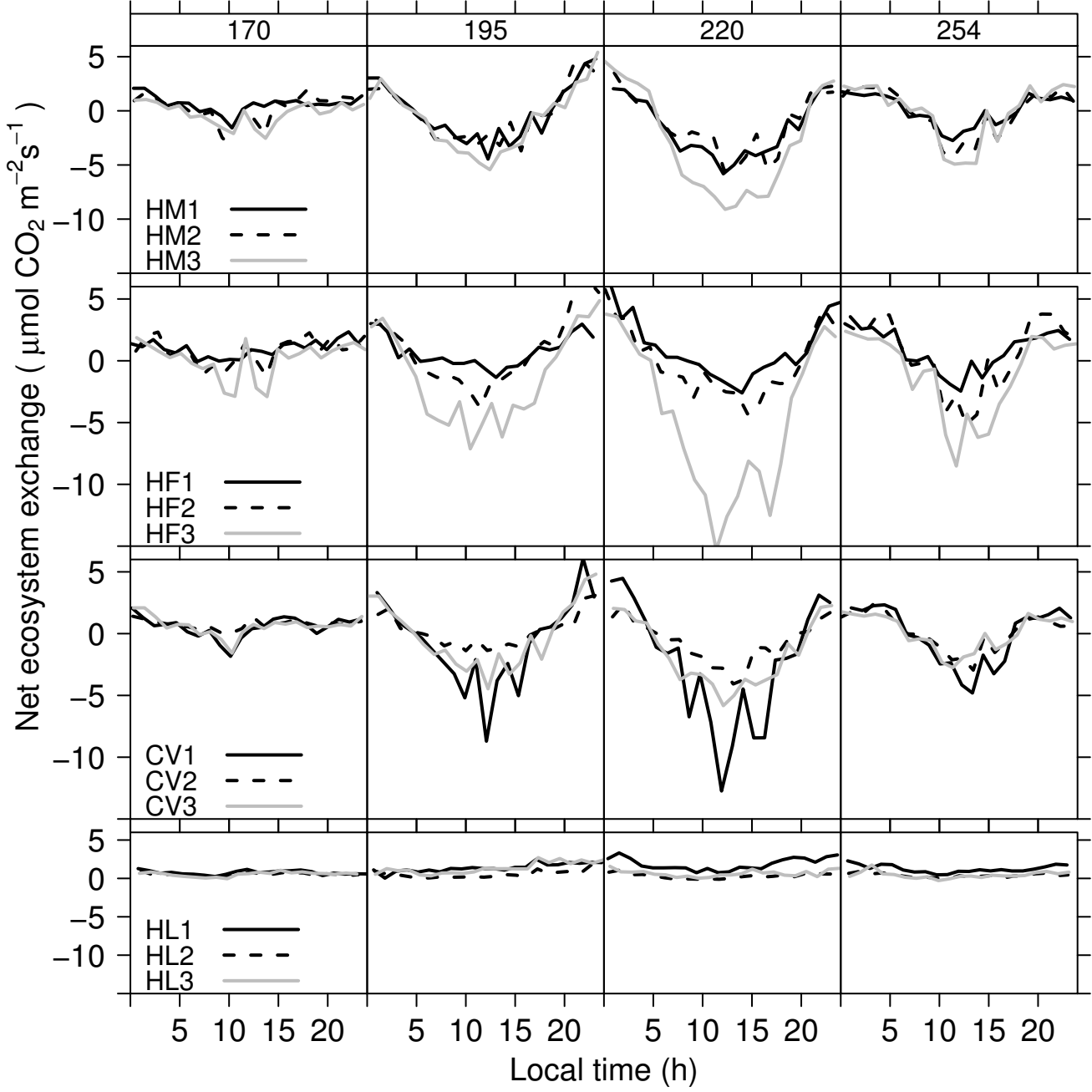
Figure 7. Relationships between growing season cumulative NEE, GPP and  $R_{eco}$  and either maximum NDVI (a, b, c) or plot LAI (d, e, f).

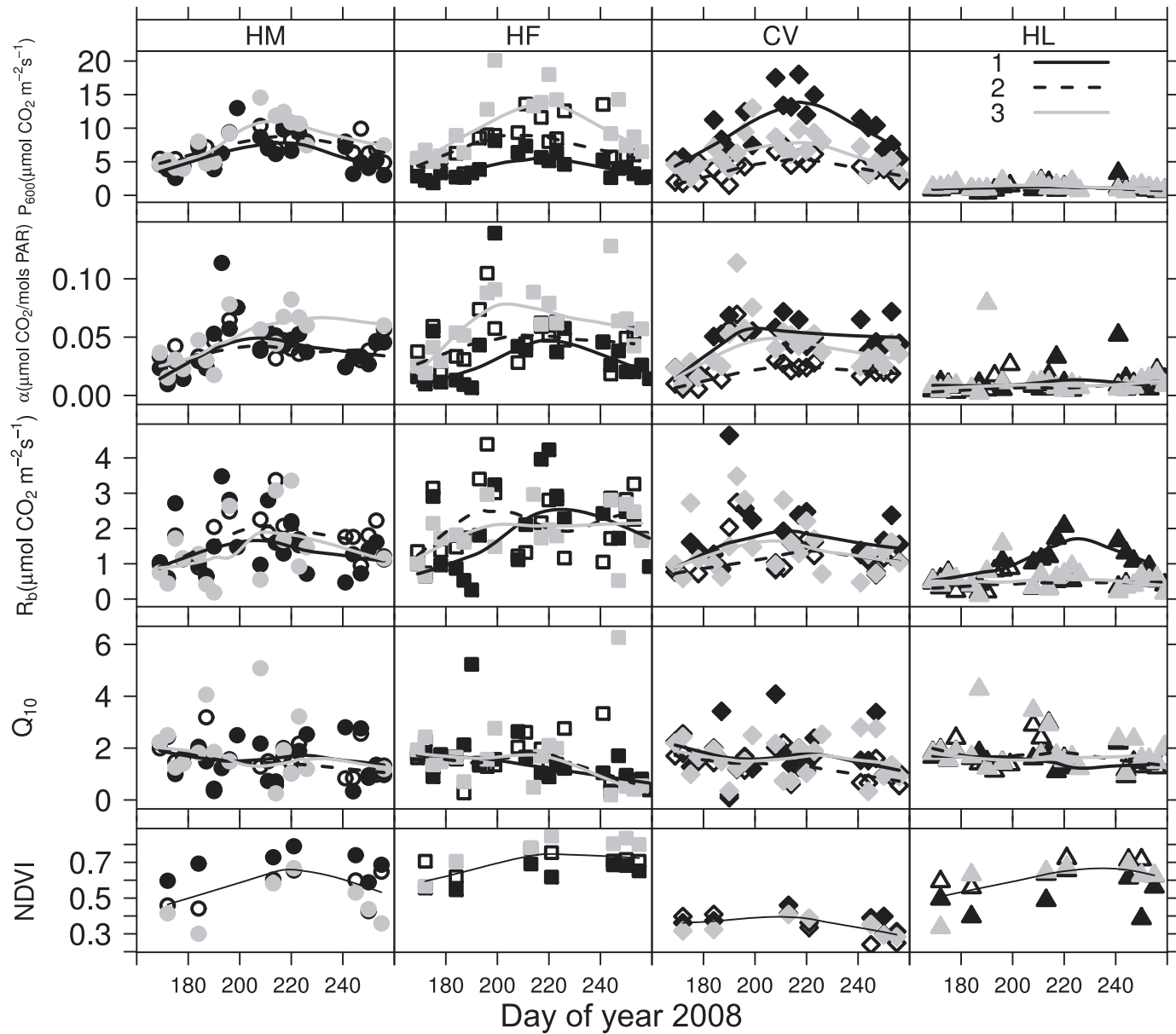
803 Figure 8. Relationship between growing season cumulative GPP and  $R_{eco}$ .

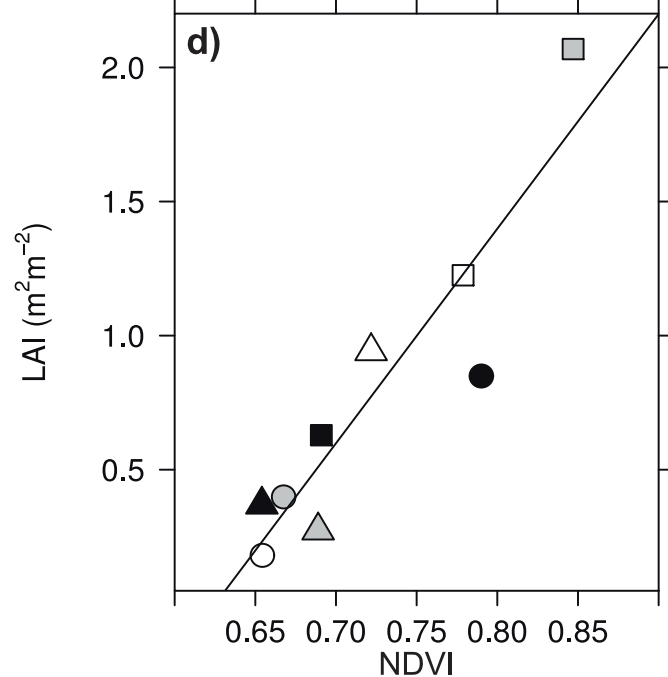
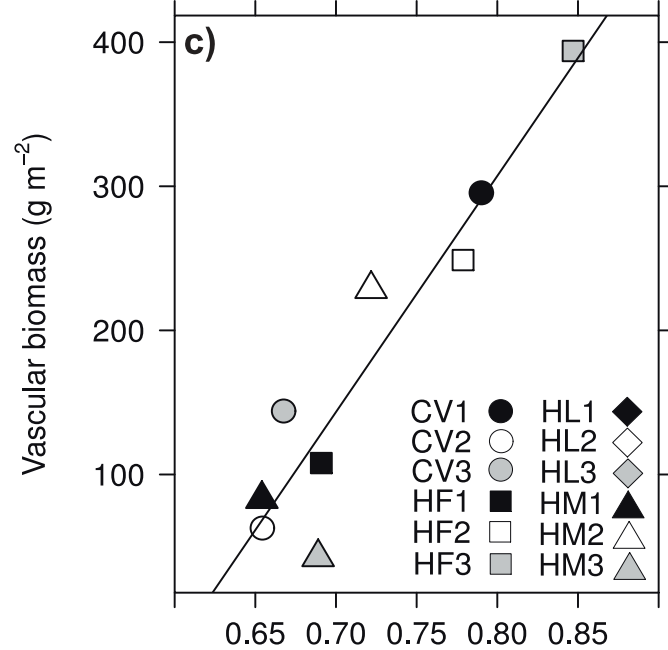
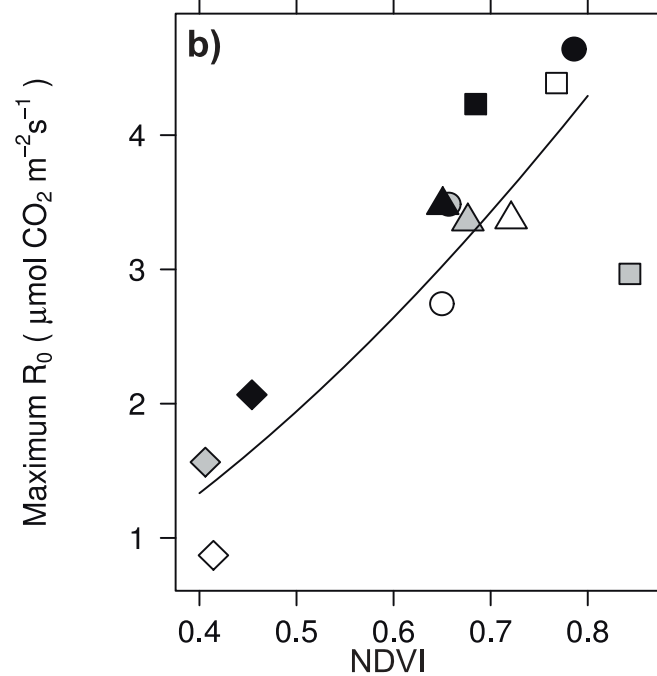
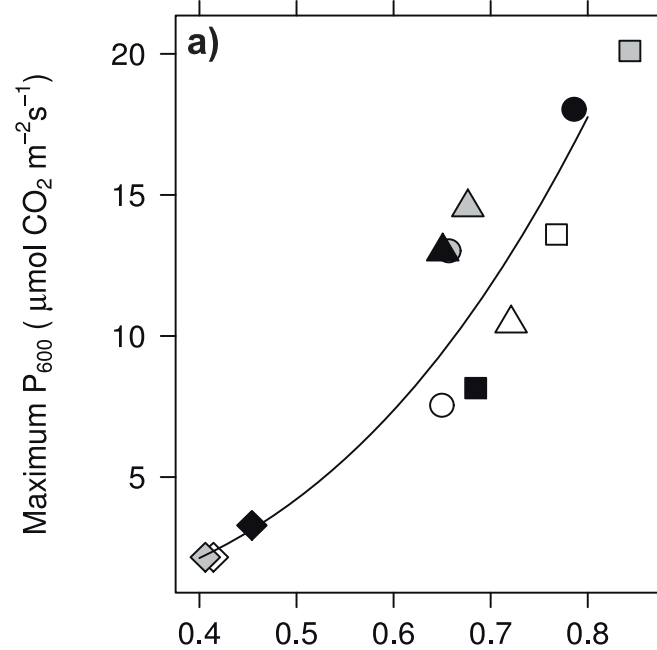
804

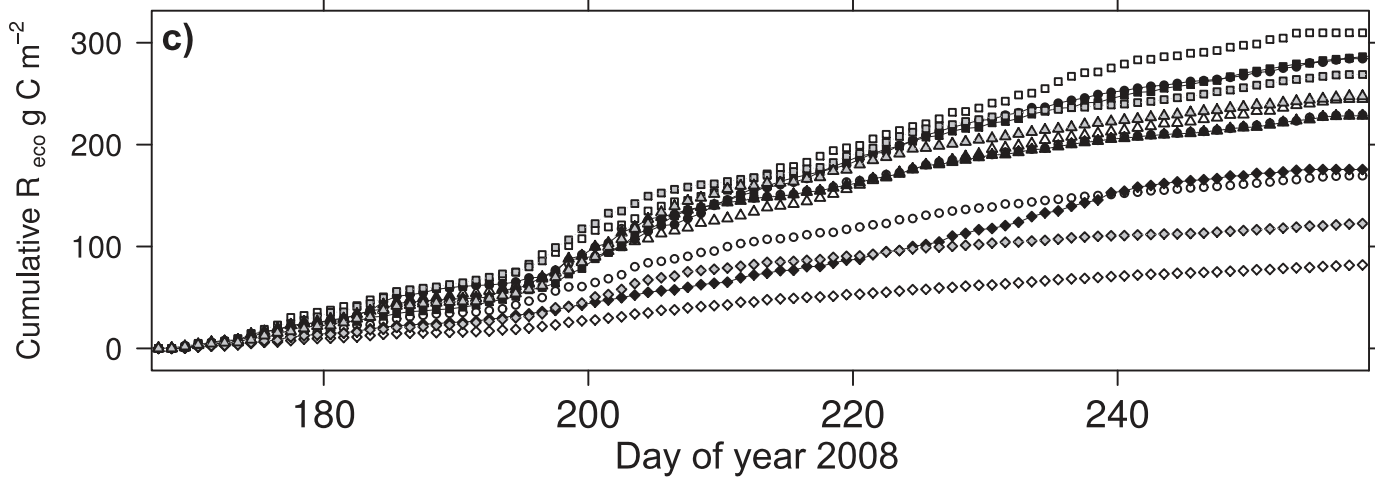
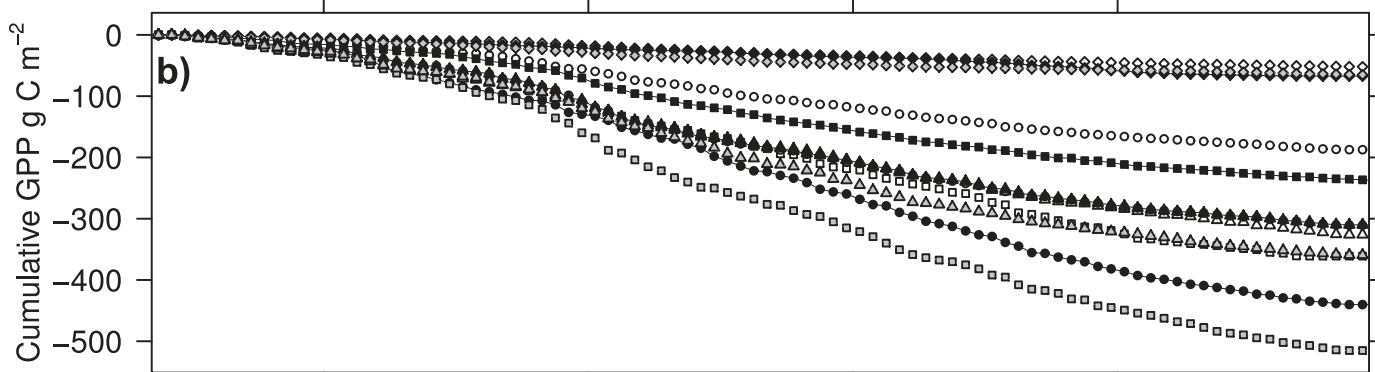
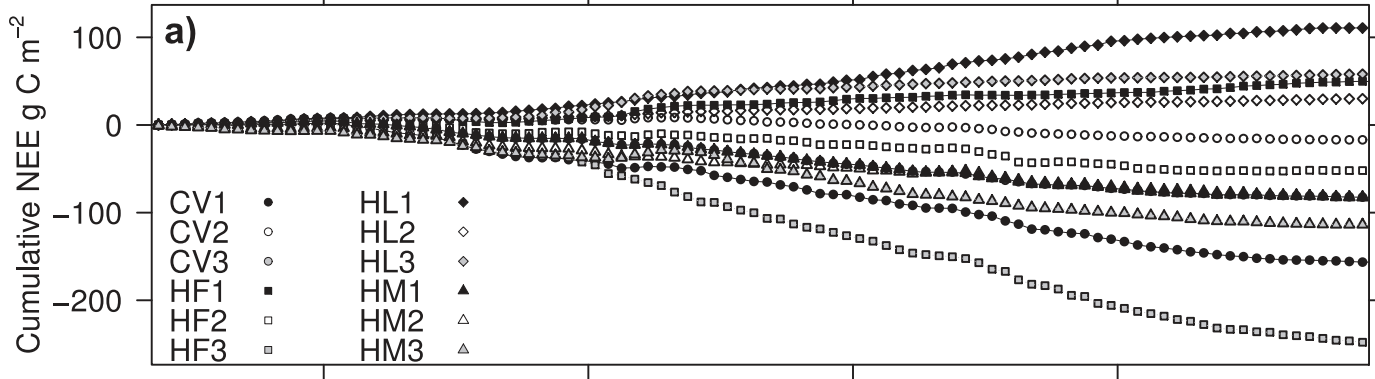




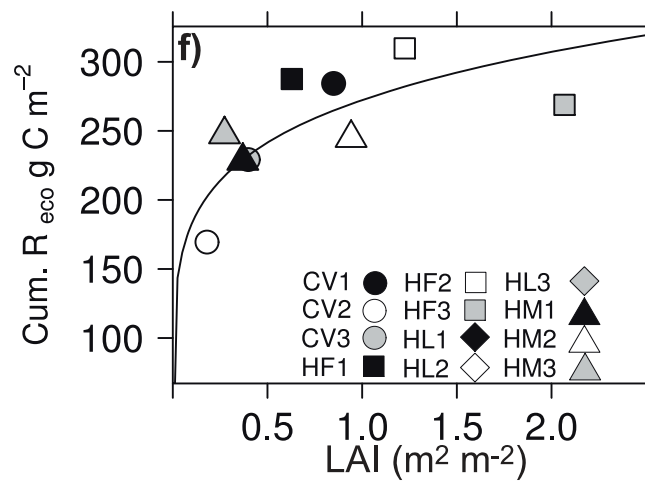
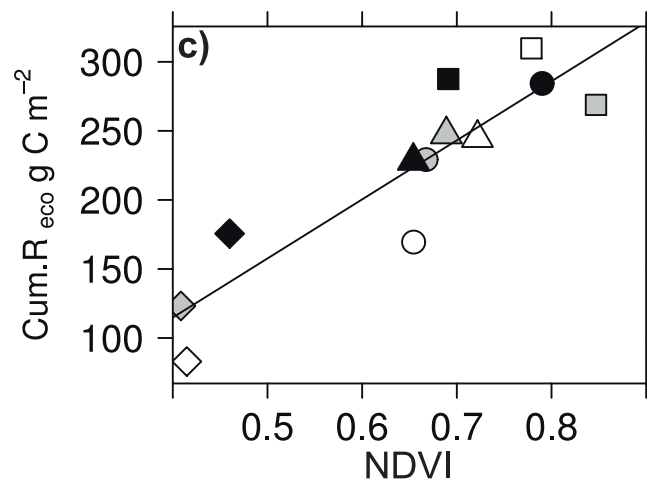
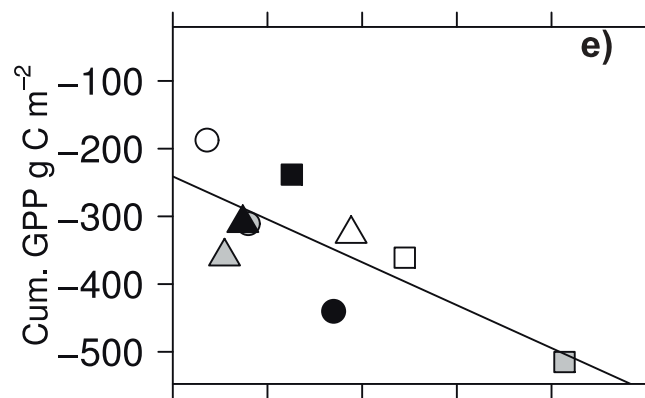
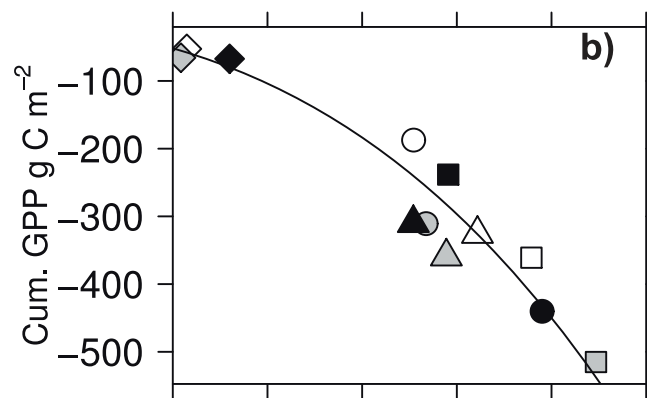
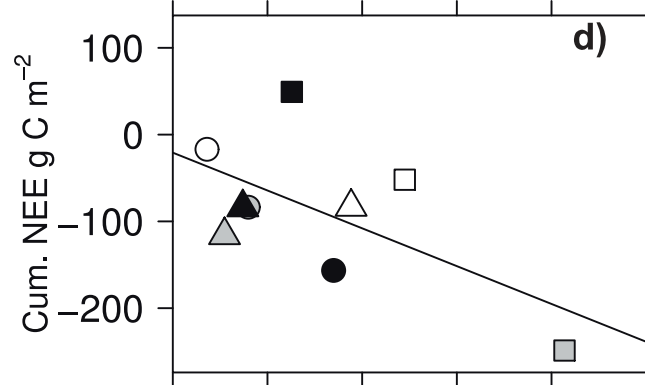
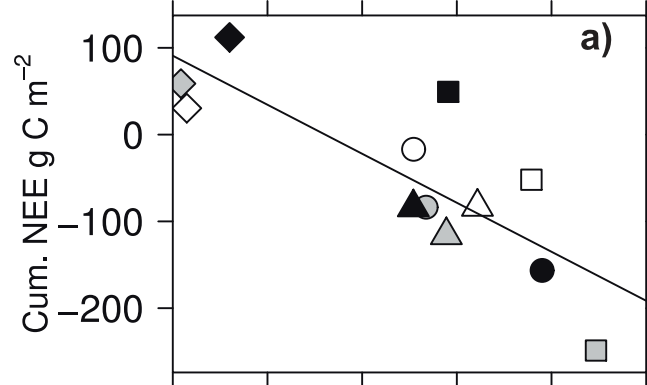


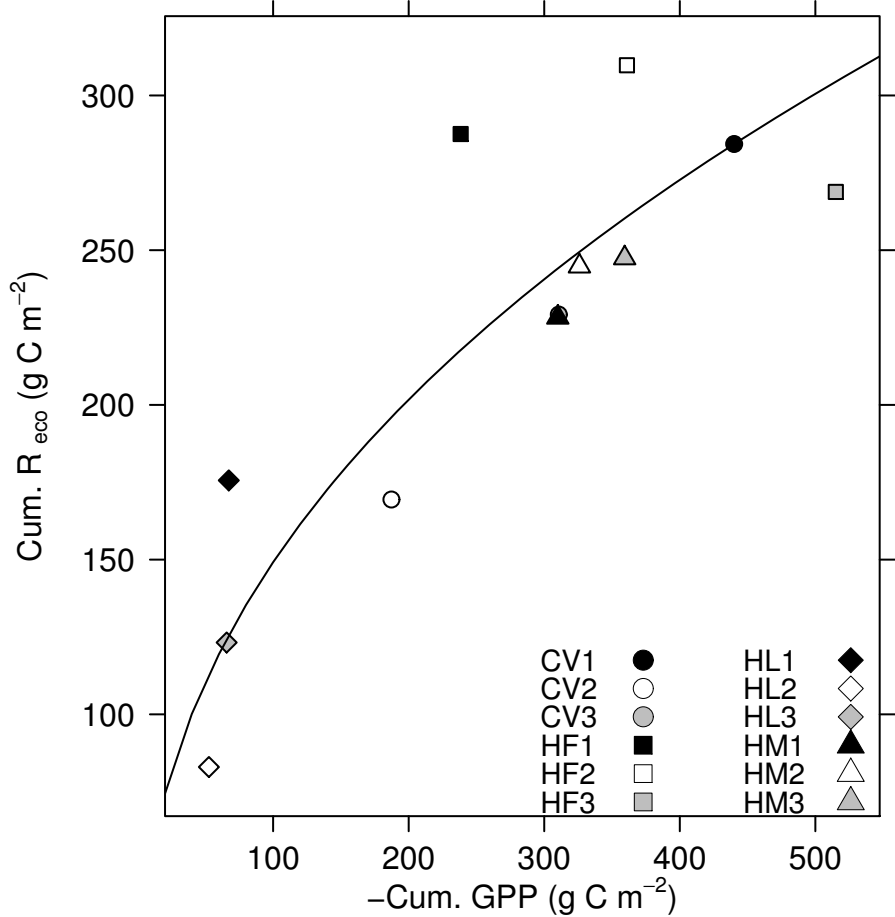












## Appendices

Appendix 1. Land classification map of the Petsikko field site, showing plot locations within the forest-mire ecotone (cf. Table 1 for the meaning of plot codes). The map is based on aerial photography taken in summer 2008 (T. Hill, unpublished). Coordinates are in UTM projection, zone 35N, datum WGS84.

Appendix 2. Statistics of the NEE model (DOY is day of year 2008).  $R_0$  is basal respiration,  $\beta$  is respiration sensitivity to temperature,  $P_{max}$  is asymptotic maximum photosynthesis,  $\alpha$  is quantum efficiency and  $P_{600}$  is gross photosynthesis at PAR = 600  $\mu\text{mol m}^{-2} \text{s}^{-1}$ . Adjusted  $R^2$  and root mean square error (RMSE) are also shown.